Microstructural characterization of U-7.5Nb-2.5Zr alloy after ageing and constrained fatigue

*Nathanael Wagner Sales Morais[a,b]** ⓘ *, Cristiano Stefano Mucsi[a], Zacarias Eduardo Fabrim[a],*

Cláudio Geraldo Schön[b], Jesualdo Luiz Rossi[a]

[a]*Instituto de Pesquisas Energéticas e Nucleares (IPEN), Centro de Ciência e Tecnologia de Materiais, Av. Prof. Lineu Prestes, 2242, Butantã, 05508-000, São Paulo, SP, Brasil.*

[b]*Universidade de São Paulo Escola Politécnica, Departamento de Engenharia Metalúrgica e de Materiais, Av. Prof. Mello Moraes, 2463, Butantã, 05508-030, São Paulo, SP, Brasil.*

U-7.5Nb-2.5Zr cladded in Zircaloy-4 is one of the most studied fuel prototypes. The Nb and Zr are added to the U to stabilize the body-centered cubic (BCC) gamma phase and grant mechanical and swelling resistance. The U-7.5Nb-2.5Zr undergoes the gamma to α″ phase transformation, generating compressive stresses due to the volume reduction. The α″ phase also can transform to a combination of $\alpha + \gamma_2$ phase (equilibrium phases), which are known to be hard and brittle. This work had the objective to test the effect of ageing the gamma to α″ phase in thermal cycling of a U-7.5Nb-2.5Zr cladded in Zircaloy-4 part. A co-laminated specimen was aged and thermally cycled in a dilatometry experiment. The samples were characterized through X-ray diffraction and metallography. The results show that the gamma to α″ phase transformations occur at the begin- ning of the initial ageing, followed by stress relief. During the cycling, the sample demonstrated non-equal thermal strains and presented fractures along with the U matrix.

Keywords: *U-7.5Nb-2.5Zr, thermal fatigue, phase transformation, fuel element.*

1. Introduction

Metallic uranium has high density, which allows to increase the amount of U^{235} inside the reactor core without the necessity of increase the enrichment which contributes to the non- proliferation policies[1]. Metallic U also presents better thermal conductivity compared to traditional ceramic fuels like UO_2 or the ones like UN^2.

Pure metallic uranium presents three allotropic forms. At the room temperature, it presents itself in the base-centered orthorhombic structure (U_α). The BCO structure presents high plasticity mainly deforming by twinning[3], but this structure also presents thermal expansion anisotropy, for example, 'a' and 'c' crystalline axis expands while 'b' axis shrinks. This behavior causes severe dimensional instability[4]. At 661 °C the pure U transforms in to a tetragonal structure (U_β), undergoing a 1% contraction. The tetragonal phase is hard to stabilize and the literature on this topic is scarce. Finally, at 769 °C, metallic U transforms into a body-centered cubic (BCC) structure (U_γ) undergoing a 0.6% volume contraction[5].

In order to solve the dimensional instability problem, alloying elements like Nb and Zr are added to U[6]. The addition of circa of 9 mass% of Nb[7] or 20 mass% of Zr[8] individually are capable of stabilize the BCC (U_γ). Both elements also enhances other properties, like Nb enhances the plasticity of the (U_γ) and the Zr increases the swelling resistance, making combinations of Nb and Zr a good solution to avoid high

alloying, which reduces the alloy density, and combining the best of their properties[6].

The addition of alloying elements also brings the possibility new phase transformations to metallic U. Low Nb additions ($\leq 3\%$) inhibits the formation of the (U_β) and causes the formation of the U_α' phase, a martensitic distortion on the (U_α) phase. Nb additions about 5.8% can lead to the precipitation of another martensitic phases, the U_α'', a monoclinic distortion of the orthorhom- bic (U_α) phase and the $U_\gamma 0$ phase, a tetragonal distortion of the (U_γ) BCC phase[9]. Zr additions below 20 mass% also causes the precipitation of martensitic U_α' phase[8]. In addition to the martensitic phases, the equilibrium $U_\gamma 2$ and $U_\gamma 3$ can precipitate after diffusional decomposition of the (U_γ). Table 1 contains a description of each U phase and system were it occurs.

The U-7.5Nb-2.5Zr, also known as Mulberry alloy, is one the U-Nb-Zr alloys studied as can- didate to fuel research reactors. This alloy presents mechanical properties that can withstand the fabrication process of the alloy and of a monolithic fuel element[11].

According to the time-temperature-transformation published by Lopes[12], the Mulberry alloy can suffer the phase transformations $\gamma \rightarrow \alpha''$ and $\gamma \rightarrow \alpha' + \gamma_3$. Both phase transformations should present volume shrinkage[12]. The first transformation is expected to occur between 390 °C and 400 °C after 10 minutes, the second transformation should occur after 100 minutes.

*e-mail: nathanaelmorais@gmail.com

Table 1. Description of the metallic U phases mentioned on this work.

Phase	System	Description
α α′ α″ β	Pure, U-Nb, U-Zr, U-Nb-Zr U-Nb, U-Zr, U-Nb-Zr U-Nb, U-Nb-Zr Pure[1]	Base-centered orthorhombic equilibrium phase Base-centered orthorhombic non-equilibrium phase Base-centered monoclinic non-equilibrium phase Tetragonal equilibrium phase
γ γ0	Pure, U-Nb, U-Zr, U-Nb-Zr U-Nb, U-Nb-Zr	Body-centered cubic equilibrium phase Body-centered tetragonal non-equilibrium phase
γ2	U-Zr	Zr-rich body-centered cubic equilibrium phase after diffusional decomposition of the $U\gamma$
γ3	U-Nb, U-Nb-Zr	Nb-rich body-centered cubic equilibrium phase after diffusional decomposition of the $U\gamma$

[1]The U_β phase can be stabilized through alloying U with Cr[10].

1.1. Monolithic fuels

The monolithic fuels consist in a foil of U alloy cladded in Zr or Al alloys. The U alloy works as fuel and the cladding protects it from the fluid on the primary circuit of a nuclear reactor. The fabrication of the monolithic fuels is performed by hot isostatic pressing (HIP)[13] or by hot rolling the fuel alloy and the cladding alloy in order to promote diffusion welding[14]. Since the U and Zr have complete solubility in the (U_γ) phase, the hot rolling is performed above the (U_γ) formation temperature, but below the transus temperature of Zr to avoid the $Zr_\beta \rightarrow Zr_\alpha$ reaction, which causes volume shrinkage and could lead to crack formation at the interface between the fuel and the cladding.

Once both alloys are bind, they must withstand the mechanical and thermal stresses together, but they have different linear thermal expansion coefficients, which can cause thermal fatigue. The open literature on thermal fatigue on monolithic fuels is scarce. Lopes performed thermal cycling of a U-10Mo foil cladded in Zircaloy-4 and observed that the alloy fracture due the strain hardening caused by the constraining[15]. The (U_γ) U-10Mo is stable at the cycled temperature range, so no phase transformation was observed by Lopes. Since there is little information on thermal fatigue of monolithic prototypes, this work presents a result of thermal cycling after ageing a of Mulberry/Zircaloy-4 monolithic fuel prototype.

2. Experimental Procedure

2.1. Sample preparation

One U-7.5Nb-2.5Zr alloy slug was Vacuum Induction melted in a carbon crucible using as raw materials natural metallic U ($U^{235} < 0.7\%$, with major impurities: 147 ppm Mn , 95 ppm Ni, 47 ppm Cu, 19 ppm Fe and 15 ppm O), sponge Zr (major impurities: 0.166 ppm Fe and 0.022 ppm Hf, 2 ppm O) and high purity Nb (major impurities: 0.14 ppm Ta, 25 ppm O). The melting procedure was similar to the one reported in the previous works of the group[16-20]. The molten alloy was then cast into a copper mold. The chemical composition of the obtained alloy was determined as U-7.4Nb-2.3Zr was measured through inductively coupled plasma - optical emission spectrometry (ICP-OES). After the casting, the samples were homogenized at 1000°C for 5h in high purity Argon atmosphere, followed by water quenching in order to stabilize the γ phase.

The Zircaloy-4 frame cladding was machined by wire electro-erosion. The covers and the frame were polished to 1 µm diamond paste. The Mulberry alloy was also polished to 1 µm diamond paste and stored in analytic ethyl alcohol. The set was assembled and welded using auto- genous gas tungsten arc welding (GTAW). The assembly was cladded in a colloidal carbon painted steel frame. The sample was hot rolled together with the Zircaloy-4 sheet using the procedure re- ported by Lopes[21], in order to fabricate a prototype of co-rolled plate.

2.2. Thermal cycling

After the hot rolling, the plate was cut in to two 5 mm x 5 mm x 2 mm pieces. The sample con- sists a 'sandwich' of U-7.5Nb-2.5Zr in Zircaloy-4, this design alloys the sample to freely expands and shrink in the normal direction, since there is no constraining in that direction. One piece was used as control sample, the other sample was placed on the thermomechanical analyzer (TMA) instrument *Setaram Multi HTC* (Setaram 20 – 1600 °C) aged for 24 h at 400 °C, then thermally cycled.

The cycles were carried in the interval 200 ° to 400 ° under high purity Ar atmosphere in a 5 K/min heating/cooling rate. The actuator of the TMA equipment was placed in contact with the Zircaloy-4 in the normal direction. The heating and cooling rate chosen in the thermal cycling allows to compare the obtained results with other dilatometric results in the literature, such the presented by Lopes[11].

2.3. Sample characterization

The treated samples were cold mounted in polymethyl methacrylate (PMMA) resin for surface preparation. Microstructural characterization was performed using optical microscopy. Samples were ground with SiC paper and mechanically polished with 1 µm diamond paste. Electropolish- ing was then carried out using an electrolyte containing 10% oxalic acid solution in water for 5 s using 2 V potential and using stainless steel as the cathode material. The same electrolyte was used for etching using 5 V potential at room temperature.

X-ray diffraction (XRD) was performed using a diffractometer with linear detector. The measurements were performed at room temperature with filtered Cu Kα radiation ($\lambda = 0.15418$ nm) in the θ /2θ mode, with 2θ range between 30º to 55º, with a 0.03º step. The U phases were identified

using models suggested by Lopes, and Rietveld refined to find a match in the XRD results[22], the Zr phases were identified using the crystallographic information file (CIF) proposed by Wyckoff[23]. Both phase identification and the peak indexation were performed using the GSAS software based on data available in literature[24].

3. Results and Discussion

3.1. Microstructural characterization of the initial condition

Figure 1a shows the initial microstructure on the interface of the of the control sample and the Figure 1b shows the initial microstructure of U matrix. The equiaxial Uγ grains shows uniform bounding with the Zircaloy-4 plate. No cracks are perceptible neither on the U matrix, interface or on the Zircaloy-4. Some inclusions are perceptible on the U matrix. The Figure 2 shows the XRD pattern for the initial condition. The diffractogram shows the presence of the BCC U_γ phase and the HCP Zr_α phase.
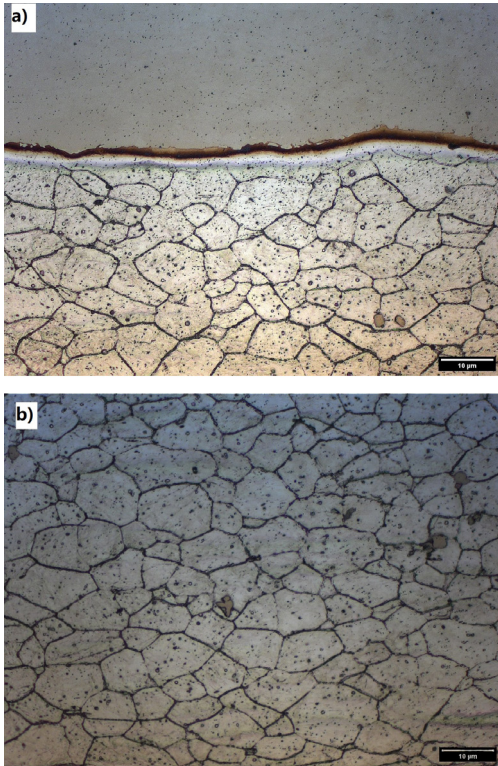
The initial microstructure is typical compared to hot rolled U_γ U-Nb-Zr alloys, as it can be seen in the literature[17,18]. No secondary phase can be seen in the uranium matrix. The X-ray diffraction confirms that there is only Zr_α and U_γ phases before the thermal cycling. The Table 2 shows the lattice parameters of the identified phases of the initial condition.

3.2. Thermal ageing and fatigue

Figure 3a shows the relative displacement of the sample during the ageing. At the beginning of the ageing, there is a strong shrinkage due the γ → α″ phase transformation. This phase transformation is expected and this behavior was previously described on the literature[11]. After 17 h, the sample presents a slight expansion ($\Delta L/L_0 < 0.001$). In the time-temperature-transformation diagram proposed by Lopes[12], the U-7.5Nb-2.5Zr alloy should undergo the γ → α′ + γ_3 phase transformation at 400 ℃ which would cause another shrinkage so, this expansion may be related to a stress relieving on the assembly.

Figure 3b shows the relative displacement of thermal fatigue. The red lines indicate the furnace temperature and the black lines indicates the relative displacement. It is important to remember that the beginning of the cycle is a cooling step, going from 400 ℃ to 200 ℃, which will cause the sample to shrink.

Since there is no constraining in the normal direction, the fatigue process occurs on the transversal and in the normal direction (shearing). Zircaloy-4, in the hexagonal close packed (HCP) structure, has a linear thermal expansion coefficient (α_T) of about 6×10^{-6} K^{-1} [25]. The linear thermal expansion coefficient of the Mulberry alloy is not reported on the literature, for instance of comparison, the linear thermal coefficient to the U_γ of the U-10 mass % Mo alloy

Figure 1. Microstructures of initial condition. (a) U-7.5Nb-2.5Zr/Zircaloy-4 interface; (b) U-7.5Nb-2.5Zr matrix.
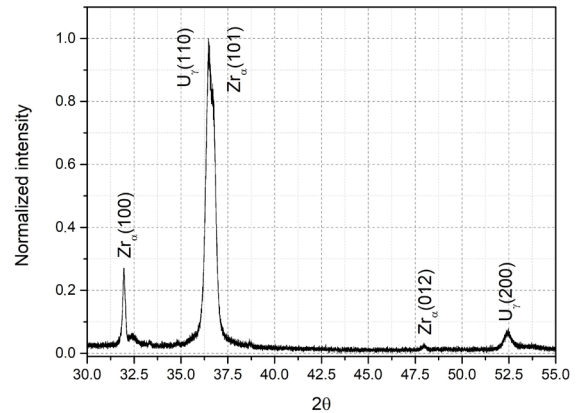
Figure 2. X-Ray diffraction pattern for the initial condition.

Table 2. Lattice parameters of the identified phases on x-ray diffraction of the initial condition sample.

Phase	Lattice parameter "a"	Lattice parameter "c"	Space group
U_γ	3.554 nm	-	I m -3 m
Zr_α	3.282 nm	5.196 nm	P 63/m m c

is $\approx 11.2 \times 10^{-6} \, K^{-1}$ [26] and Kaity fitted the dilatometric curve of the water quenched U-6 mass% $(U_\alpha'') \frac{\Delta L}{L_0} (\%) = -0.258 + 0.599 \times 10^{-3} T + 0.867 \times 10^{-6} T^{-2}$. In both cases ($U_\gamma$ or (U_α''), the thermal cy- cling would cause one material expand more than the other, creating the shearing stress to nucleate and propagate cracks.

In order to better visualize the difference between cycles, Figure 3c shows the amplitude of the cooling, heating and the residual strain after each complete cycle. Only cycles 5 and 6 presents zero residual strain. From the first to the last cycle, there is the tendency of negative residual strain, which indicated that the sample expanded a little more at each cycle, which could be indicative of the crack propagation. After the final cycle, the sample conserves a -0.0085 mm shrinkage.
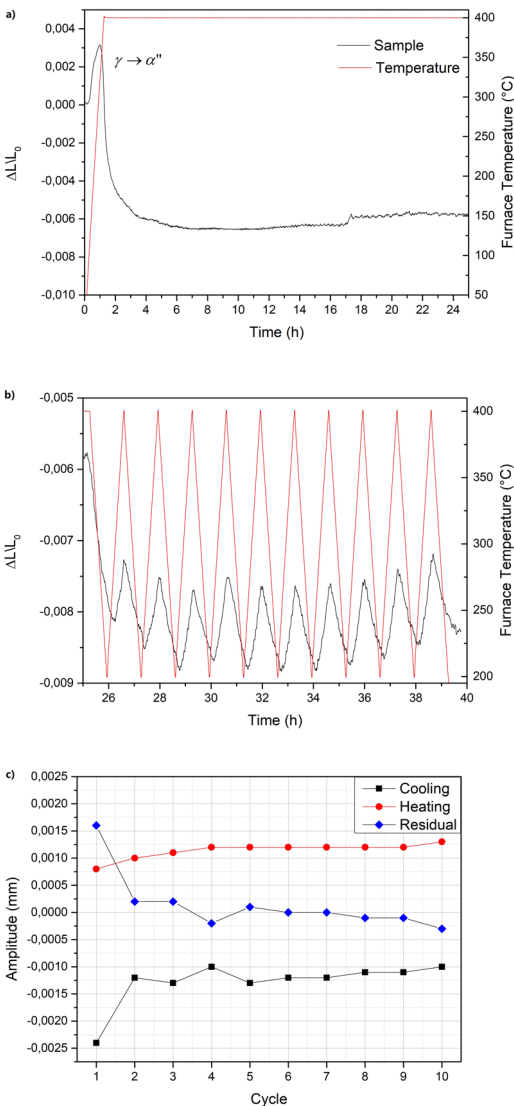
Figure 3. Results from1t0he cycling experiments. (a) Relative displacement (ΔL/L0) for the ageing heat treatment; (b) Relative displacement (ΔL/L0) for the thermal cycling; (c) Amplitude of each heating and cooling cycle. The blue dots represent the residual strain after each cycle.

3.3. Microstructural characterization of the final condition

Figure 4a presents the microstructure of the U matrix and Figure 4b presents the microstructure on the interface after the cycling. The U matrix presents a long crack perpendicular to the normal direction and a fully transformed U_α'' matrix. The interface shows no visible cracks in the Zircaloy-4 or in the interdiffusion layer, but show some cracks on the U matrix.

The microstructures of U_α'' can present itself in the accicular[18], banded and discontinuous morphology[12] depending the alloy composition and the process that generates it. The presented microstructure corresponds to the accicular form, but presenting distorted deformation bands, sheared on the horizontal direction in reference of the image, indicating that the structure was submitted to shearing and/or tearing stresses during the thermal cycling.

Based on the microstructure and in the dilatometric results, the stresses during the ageing and thermal cycling can be exemplified in the Figure 5. The initial phase transformation introduces a strong compressing stress in the normal direction. This compressing stress hinders the crack open- ing in the normal direction, the stress release generates the expansion before the cycling. Since there is no constraining in the normal direction, there is no stresses applied on the normal direction during the thermal cycling. The thermal expansion and thermal shrinkage applies only shearing and tearing stresses on the
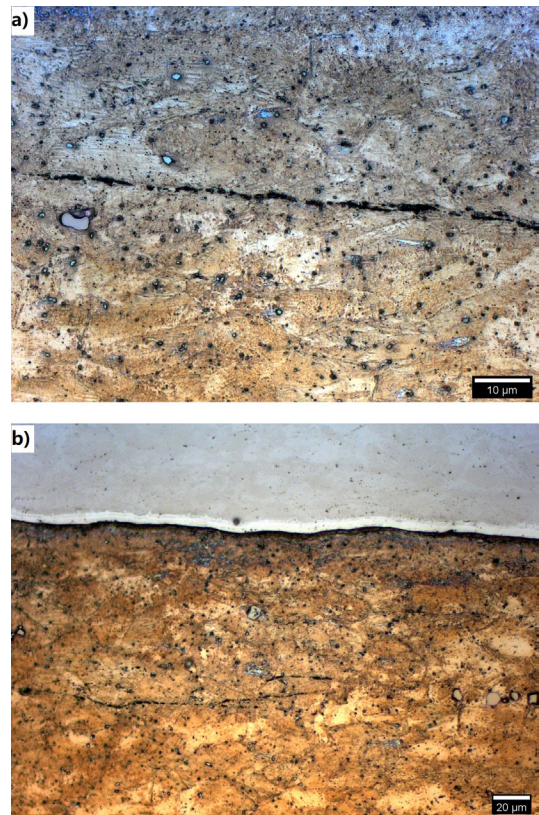
Figure 4. Microstructure of the sample after the ageing and thermal cycling. (a) U-7.5Nb-2.5Zr matrix after ageing and thermal cycling; (b) U-7.5Nb-2.5Zr / Zircaloy-4 interface after ageing and thermal cycling.

Table 3. Lattice parameters of the U_{α}'' after the thermal cycling.

Phase	Lattice Parameter "a"	Lattice Parameter "b"	Lattice Parameter "b"	Lattice Parameter "b"	Lattice Parameter "b"	Space group
U_{α}''	2.860 nm	5.882 nm	4.996 nm	90°	91.684°	C 1 1 21/m
$U_{\alpha}''_{\ reference}$ [22]	2.85 nm	5.75 nm	4.98 nm	90°	92.5°	C 1 1 21/m
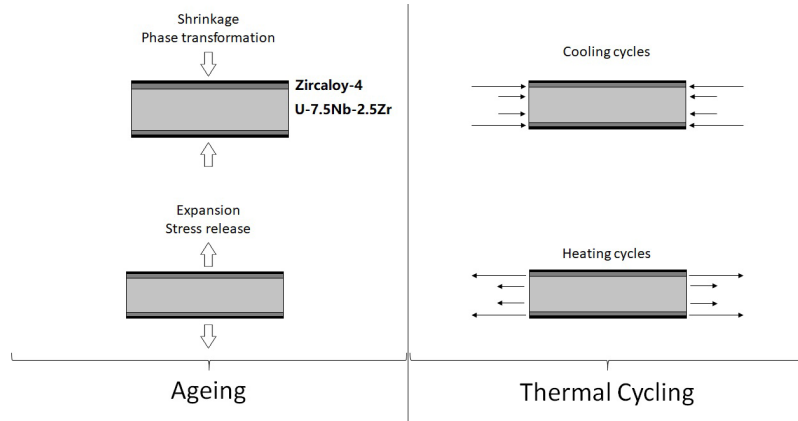
Figure 5. Stresses during the ageing and thermal cycling on the sample.
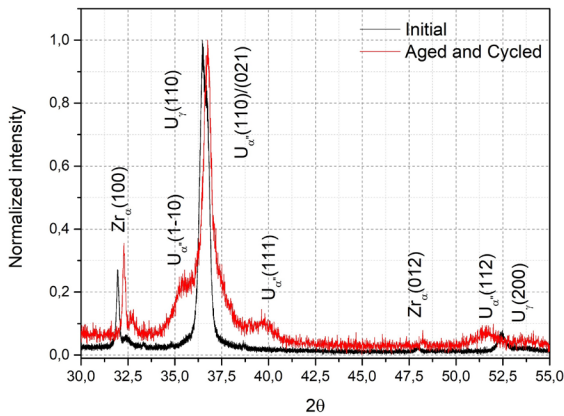
Figure 6. X-Ray diffraction pattern after the cycling.

The Table 3 shows the lattice parameters calculated for $U\alpha''$ phase. As expected, it varies from the literature reference, probably due the stresses on the structure generated by the thermal cycling.

4. Conclusions

This work performed the ageing of a Mulberry alloy cladded in Zircaloy-4 at 400 °C for 24 h followed by 10 thermal cycles in the 400 °C to 200 °C temperature range. The objective of this work was evaluate how the assembly would perform under the stress provided by difference of the linear thermal expansion coefficients. The following conclusions can be drawn:

- The ageing at 400 °C for 24 h caused a complete $\gamma \rightarrow \alpha''$ phase transformation, but was not enough to cause the $\alpha'' \rightarrow \alpha' + \gamma_3$ reaction;
- In the presented conditions ageing cycling the cracks tended to initiate perpendicular to normal direction on the U matrix, but no crack was visible on the Zircaloy-4 or in the inter- diffusion layer;
- The amplitude variation can be an indicative of crack propagation.

5. Acknowledgments

sample. Since the Zircaloy-4 has greater linear thermal expansion than the U_{α}'' in the matrix, it might generate cumulative strain hardening, as proposed by Lopes[21] to happen in the U_{γ} phase of the U-10Mo alloy in similar conditions. Once the matrix reaches the limit of strain hardening, the stresses causes the crack nucleation and propagation.

Figure 6 shows the superposition of the X-Ray diffraction pattern of the control sample and of the cycled sample. The Zr_{α} peaks shows displacement, but does not present any of the Zr_{β} peaks. The displacement could be related to the residual strain due the cycling. The results shows strong U_{α}'' peaks, but shows no peaks for U_{α}' or any U_{γ} variation, indicating that the cycling process occurred in the U_{α}'' phase.

6. References

1. Sun K, Dave AJ, Hu LW, Wilson EH, Phan S, Jaluvka D. Transitional cores and fuel cycle analyses in support of mit reactor low enriched uranium fuel conversion. Prog Nucl Energy. 2020;119:103171. http://dx.doi.org/10.1016/j. pnucene.2019.103171.

2. Keiser DD, Hayes SL, Meyer MK, Clark CR. High-density, low-enriched uranium fuel for nuclear research reactors. JOM. 2003;55:55-8. http://dx.doi.org/10.1007/s11837-003-0031-0.

3. Cahn R. Plastic deformation of alpha-uranium; twinning and slip. Acta Metall. 1953;1:49-70. http://dx.doi.org/10.1016/0001-6160(53)90009-1.

4. Kelman LR. Dimensional changes in uranium under thermal cycling. USA: National Laboratory; 1949. Technical Report ANL - FF - 54. Ar- gonne. http://dx.doi.org/10.2172/1133923.

5. Blackburn W. $\alpha - \beta$ thermal cycling of uranium. J Nucl Mater. 1960;2:191. http://dx.doi.org/10.1016/ 0022-3115(60)90049-0.

6. Ghoshal K, Kaity S, Mishra S, Kumar A. Microstructural investigation of uranium rich U – Zr – Nb ternary alloy system. J Nucl Mater. 2014;446:217-23. http://dx.doi.org/10.1016/j. jnucmat.2013.12.015.

7. Justusson W. Transformation kinetics of gamma-phase uranium molybdenum-niobium alloys. J Nucl Mater. 1961;4:37-45. http://dx.doi.org/10.1016/0022-3115(61)90147-7.

8. Basak CB, Prabhu N, Krishnan M. On the formation mechanism of the UZr_2 phase. Intermetallics. 2010;18:1707-12. http://dx.doi.org/10.1016/j.intermet.2010.05.006.

9. Zhang Y, Zhang X, Chen X, Weijun G, Wang X. Effect of grain size on phase stability of monoclinic U – Nb alloy during low-temperature aging. J Nuclear Mater. 2015;465:167-9. http://dx.doi.org/10.1016/j.jnucmat.2015.05.020.

10. Donohue J, Einspahr H. The structure of beta-uranium. Acta Crystallogr B. 1971;27:1740-3.

11. Lopes DA, Restivo TAG, Padilha AF. Mechanical and thermal behaviour of U – Mo and U – Nb – Zr alloys. J Nucl Mater. 2013;440:304-9. http://dx.doi.org/10.1016/j.jnucmat.2013.05.014.

12. Lopes DA, Restivo TAG, Padilha AF. Phase transformation studies in u–nb–zr alloy. Nucl Eng Des. 2013;265:619-24. http://dx.doi.org/10.1016/j.nucengdes.2013.09.024.

13. Park Y, Eriksson N, Newell R, Keiser D, Sohn Y. Phase decomposition of γ-u (bcc) in u-10 wt% mo fuel al- loy during hot isostatic pressing of monolithic fuel plate. J Nucl Mater. 2016;480:271-80. http://dx.doi.org/10.1016/j.jnucmat.2016.08.022.

14. Gan J, Miller BD, Keiser DD Jr, Jue JF, Madden JW, Robinson AB, et al. Irradiated microstructure of u-10mo monolithic fuel plate at very high fission density. J Nucl Mater. 2017;492:195-203. http://dx.doi.org/10.1016/j.jnucmat.2017.05.035.

15. Lopes DA, de Oliveira Zimmermann AJ, Restivo TAG, Padilha AF. Hardness response surface for U-7.5Nb-2.5Zr alloy: a study of recovery/recrystallization and phase transformation interactions. Metall. Mater. Trans. E. 2015;2:147-56. http://dx.doi.org/10.1007/s40553-015-0052-y.

16. Morais NWS, Lopes DA, Scho¨n CG. Effect of thermo-mechanical processing on microstructure and mechanical properties of U – Nb – Zr alloys: Part 1 - U – 6 wt. % Nb – 6 wt. % Zr. J Nucl Mater. 2017;488:173-80. http://dx.doi.org/10.1016/j. jnucmat.2017.03.006.

17. Morais NW, Tunes MA, Santos VO, Gomide RG, Schon C. Influence of zr, mo and nb on microstrucutre of ternary uranium alloys. In: 2015 TopFuel Conference; 2015; Brussels, Belgium. Proceedings. Brussels, Belgium: European Nuclear Society; 2015. Poster.

18. Morais NWS, Lopes DA, Scho¨n CG. Effect of thermo-mechanical processing on microstructure and mechanical properties of U – Nb – Zr alloys: Part 2 - U – 3 wt % nb – 9 wt % Zr and U – 9 wt% Nb – 3 wt% Zr. J Nucl Mater. 2018;502:51-9. http://dx.doi.org/10.1016/j.jnucmat.2018.01.045.

19. Morais NWS. Influência dos teores de Nb e Zr e do processamento na microestrutura e propriedades mecânicas de ligas U-Nb-Zr [thesis]. São Paulo: Universidade de São Paulo; 2018.

20. Morais NWS, Schön CG. Laves phases in the U – Mo – Zr system. J Alloys Compd. 2020;863:158070. http://dx.doi.org/10.1016/j.jallcom.2020.158070.

21. Lopes DA, Zimmermann AJ, Silva SL, Piqueira J. Thermal cycling effect in U-10Mo/Zry-4 monolithic nuclear fuel. J Nucl Mater. 2016;473:136-42. http://dx.doi.org/10.1016/j. jnucmat.2016.02.029.

22. Lopes DA. Interação entre precipitação e recristalização em liga de urânio contendo nióbio e zircônio (Mulberry alloy) [thesis]. São Paulo: Universidade de São Paulo; 2013. http://dx.doi.org/10.11606/T.3.2013.tde-29102014-171203.

23. Wyckoff RWG. Crystal structures. Vol. 1. 2nd ed. New York: Interscience Publishers; 1963.

24. Toby BH, Von Dreele RB. Gsas-ii: the genesis of a modern open-source all purpose crystallography software package. J Appl Cryst. 2013;46:544-9. http://dx.doi.org/10.1107/S0021889813003531.

25. AZO Materials. Zircaloy-4(alloy zr4) (uns r60804) data sheet [Internet]. Manchester: AZO Materials; 2013. [cited 2023 Jan 14]. Available from: https://www.azom.com/article.aspx?ArticleID=7644.

26. Burkes D, Mickum G, Wachs D. Thermo-physical properties of U-10Mo alloy. USA: Idaho National Laboratory; 2010. Technical Report, INL/EXT-10-19373.